JACS
JOURNAL OF THE AMERICAN CHEMICAL SOCIETY

Communication

pubs.acs.org/JACS

Dynamic Tuning of DNA-Nanoparticle Superlattices by Molecular Intercalation of Double Helix

Suchetan Pal,[†,‡] Yugang Zhang,[‡] Sanat K Kumar,[†] and Oleg Gang*[,‡]

[†]Department of Chemical Engineering, Columbia University, New York City, New York 10027, United States
[‡]Center for Functional Nanomaterials, Brookhaven National Laboratory, Upton, New York 11973, United States

Supporting Information

ABSTRACT: Nanoparticle (NP) assembly using DNA recognition has emerged as a powerful tool for the fabrication of 3D superlattices. In addition to the vast structural diversity, this approach provides an avenue for dynamic 3D NP assembly, which is promising for the modulation of interparticle distances and, hence, for example, for *in situ* tuning of optical properties. While several approaches have been explored for changing NP separations in the lattices using responsiveness of single-stranded DNA (ss-DNA), far less work has been done for the manipulation of most abundant double-stranded DNA (ds-DNA) motifs. Here, we present a novel strategy for modulation of interparticle distances in DNA linked 3D self-assembled NP lattices by molecular intercalator. We utilize ethidium bromide (EtBr) as a model intercalator to demonstrate selective and isotropic lattice expansion for three superlattice types (bcc, fcc, and AlB_2) due to the intercalation of ds-DNA linking NPs. We further show the reversibility of the lattice parameter using *n*-butanol as a retrieving agent as well as an increased lattice thermal stability by 12−14 °C due to the inclusion of EtBr. The proposed intercalator-based strategy permits the creation of reconfigurable and thermally stable superlattices, which could lead to tunable and functionally responsive materials.

Synthetic deoxyribonucleic acid (DNA) is now widely demonstrated as a powerful tool for self-assembly of plasmonic nanoparticles (NPs) into discrete, 1D, 2D, and 3D architectures due to its unique programmable interactions.[1,2] Particularly, DNA directed self-assembly of NPs into 3D superlattices has achieved many advances after its advent in 2008.[3,4] Through careful selection of overall particle size, shape, and composition, it is now possible to create a vast library of self-assembled NP superlattices, which incorporate elements of multiple types.[5−8]Those macroscopic aggregates have shown immense potential as optically active or multicomponent metamaterials.[9,10]

Recently, there has been a great deal of interest for building dynamically tunable, self-assembled nanostructures which are able to change their physical and/or chemical properties upon the application of external stimuli. Polymeric materials have been extensively used for this purpose due to their structural responsiveness to the chemical modifications or external stimuli.[11] Since polymers and biopolymers are advantageous for controlling NP organizations, such responsiveness can be further utilized for creating adaptive NP systems.[12] In particular, DNA-linked NP systems have attracted significant attention in recent years. The low persistence length of single-stranded DNA (ss-DNA), its charged backbone, and readiness to hybridize to complementary strand make DNA a convenient platform for dynamically reconfigurable 3D superlattices.[13−20] It has been shown that the interparticle distances can be modulated using pressure, humidity, salt concentration, or changes in NP DNA shells.[13−22] These structural reconfigurations of NP superlattices allow fine-tuning of separations between plasmonic NPs, which, in turn, modulates the optical properties.[17,18] However, it remains challenging to establish a simple, yet broadly applicable approach for the modulation of interparticle distances in the most abundant and structurally defined double-stranded DNA (ds-DNA) forms. Such an approach might significantly broaden the use of DNA-guided NP superlattices for the creation of system with tunable functions.

Herein, we demonstrate a strategy based on the intercalation of a small molecule into ds-DNA for achieving reversible distance modulation with nanometer scale precision. We use EtBr as a model intercalator in this study. Although EtBr has been used extensively for DNA staining in molecular biology, only recently it has been utilized in structural DNA nanotechnology as a tool for the relief of the helical twist in strained DNA origami structures, as well as a molecular chaperone.[23,24] The intercalation property of EtBr makes it an excellent candidate for manipulation of ds-DNA motifs between NPs. EtBr is a flat, π-electron-rich molecule shown in Figure 1, with a positive charge, which enables the molecule to slide in between base pairs (bp) in a ds-DNA molecule via $\pi-\pi$ stacking interactions, inducing a 0.34 nm distance and 26° of twist relief per EtBr molecule.[25,26] We sought to utilize this EtBr intercalation feature for modulating interparticle distances in NP superlattices, where particles are connected by predominantly ds-DNA motifs (Figure 1). When the preformed DNA-NP superlattices are exposed to the EtBr molecules, ds-DNA becomes permeated and intercalated, resulting in the lattice expansion. Due to the relative uniform distribution of larger numbers of ds-DNA on NP surface, we hypothesized that the expansion would be isotropic.

To experimentally demonstrate the aforementioned concept, we first fabricated the body-centered cubic (bcc) NP superlattices using a previously described method (SI, section 3.1 for details).[5] Gold nanoparticles (AuNPs) with a core diameter (d) of ∼10 nm were functionalized with two different thiolated ss-

Received: December 16, 2014
Published: March 9, 2015

DOI: 10.1021/ja512799d
J. Am. Chem. Soc. 2015, 137, 4030−4033

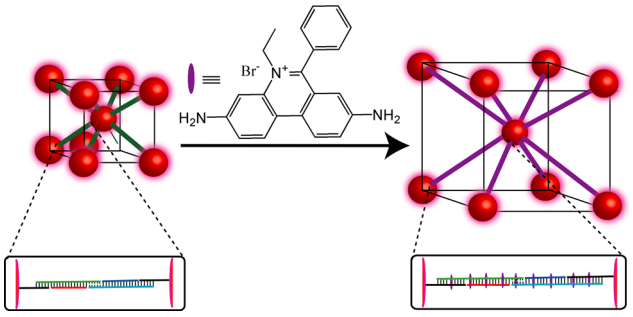

Figure 1. Schematic description of EtBr-based interparticle distance modulation in 3D NP superlattices. AuNPs (red spheres) are connected by ds-DNA linker. EtBr (purple disks) can slide in between neighboring base pairs using stacking interactions which enlarges ds-DNA length, and therefore the interparticle distance increases.

DNA, denoted as A and B, respectively. We then hybridized two different types of ds-DNA linkers to each of the A and B AuNPs. The linker DNA has three distinct binding regions depicted in Figure 2a: (i) a ss binding region, A- or B-bind for the attachment

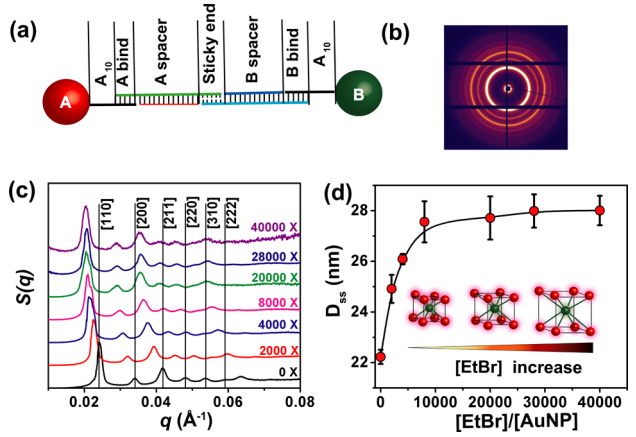

Figure 2. (a) NP linker design for bcc superlattice. (b) Representative SAXS pattern for bcc superlattice. (c) Evolution of the structure factor $S(q)$ for bcc superlattices with increasing excess of EtBr with respect to the particle concentration (25 nM). Diffraction peaks in $S(q)$ for native (without EtBr) superlattice are indexed (as shown) with bcc planes (black vertical line). The diffraction peaks shift to lower q, indicating the D_{CC} increase. See Figure S19 for enlarged view. (d) The surface-to-surface separations, D_{SS}, for the same system, as obtained from the SAXS measurements with respect to [EtBr]/[AuNP], where [EtBr] and [AuNP] are the concentrations of EtBr and AuNP, respectively.

of the linker to the ss-DNA grafted on A or B AuNPs, (ii) a variable ds-spacer region, A- or B-spacer, and (iii) a 6 bp sticky end for the interparticle binding. The interparticle distances can be controlled by changing the length of A or B spacer. We determined that each AuNP has ≈80 ds linkers. The final assembly process was performed by equimolar mixing of A and B particles, following by a thermal cycling from 40 to 30 °C, which is required for the formation of the crystalline phase. Complementary DNA-coated NP of similar core and shell sizes typically forms a bcc superlattice, where one A particle is connected to eight B particles and vice versa. For the initial verification of the proposed approach, we started with a bcc superlattice containing 72 bp in the dsDNA motif and 20 bases (b) ss-DNA motif linking two particles, as shown in Figure 2a. The formation of bcc phase was verified by small-angle X-ray scattering (SAXS) experiments at X9 beamline at NSLS (BNL) from the assembled aggregates in a buffered solution. The structure factor, $S(q)$ was derived from azimuthal integration of intensity of a typical SAXS image (Figure 2b).[3] The 1D intensity plot exhibited several orders of diffraction peaks at $q_n/q_1 = 1:\sqrt{2}:\sqrt{3}:\sqrt{4}$ ratio in wave vector (q) axes, where q_n is the position of nth order peaks. This observation confirmed the formation of a highly ordered bcc lattice as indexed in Figure 2c (black vertical lines). The interparticle center-to-center distance, D_{CC}, obtained from SAXS experiments $D_{CC} = ((\sqrt{6\pi})/(10 \times q_1)) \approx 32.4$ nm agrees well with the expected distance 33.7 nm, based on an average 0.255 nm per base pair, observed for similar shells.[5] The well-ordered bcc superlattice was then subjected to further experiments.

Since more than 80% of the volume of 3D NP superlattice is occupied by water, its internal space can be accessed by external chemical signals without imposing osmotic pressure, if such molecules are smaller than the DNA mesh size.[3,15] The relatively open environment of DNA-NP lattice permits a small organic molecule, like EtBr, to penetrate and intercalate the ds-DNA linkers. In order to demonstrate this, we added increasing amounts of EtBr into the preassembled bcc superlattices and probed the structure using *in situ* SAXS experiments. Our time dependent structural measurements indicate that the intercalation process took less than 6 min to complete (the time required for probing in our setup) after the addition of EtBr (see Figure S13). We observed that upon EtBr concentration increase the positions of the scattering peaks gradually shifted to lower q values, as shown in Figure 2c. However, the relative positions of the peaks q_n/q_1 were not affected, indicating that the structural integrity remained intact during the intercalation process. D_{CC} gradually increased from ∼32.4 to 38 nm. Since the AuNP core size is constant during the intercalation process, the changes in D_{CC} can be attributed to the expansion of NP's DNA shell. The surface-to-surface separation between neighboring NPs in the superlattice, D_{SS} ($D_{SS} = D_{CC} - d$, where d is the diameter of gold core) monotonically increased with EtBr concentration. In our experiment, D_{SS} increased from ≈22.4 to ≈28.0 nm with [EtBr]/[AuNP] increased to 40000, as depicted in Figure 2d. D_{SS} shows a saturation behavior at higher [EtBr]/[AuNP](>10000). These observations demonstrate that EtBr intercalation in DNA has a profound effect on D_{SS} at low EtBr concentrations. However, at higher EtBr concentrations, the binding and corresponding structural changes became limited due to the reduced availability of intercalating sites on ds-DNA. Considering that the size of EtBr is approximately the same as nucleobases and neglecting the effect of EtBr on ss-DNA (as we discuss below), we estimate ∼23 intercalating molecules per 72 bp ds region (i.e., ≈1 EtBr molecules/3bp). This value agrees with the data for free ds-DNA.[25]

We further investigated if our lattice modulation approach can be used for other types of DNA-NP superlattices. In addition to bcc, we created face-centered cubic (fcc) and AlB_2 superlattices using a previously published protocol.[5] For fcc lattice, a 5 nm AuNP, denoted as C, was grafted with ss-DNA, following the linker attachment. The linker has two distinct regions as shown in Figure 3a, namely, (i) C-bind and (ii) a self-complementary sticky end region (SI, section 3.2 for details). Only one type of NP was used to assemble the fcc structure. Each NP in the fcc lattice is identical and connected to 12 equidistant neighbors separated by a total of 76 bp ds- and 10 b ss-DNA motifs. The formation of the fcc lattice, following system assembly and annealing, was confirmed by *in situ* SAXS measurements. A

DOI: 10.1021/ja512799d
J. Am. Chem. Soc. 2015, 137, 4030−4033

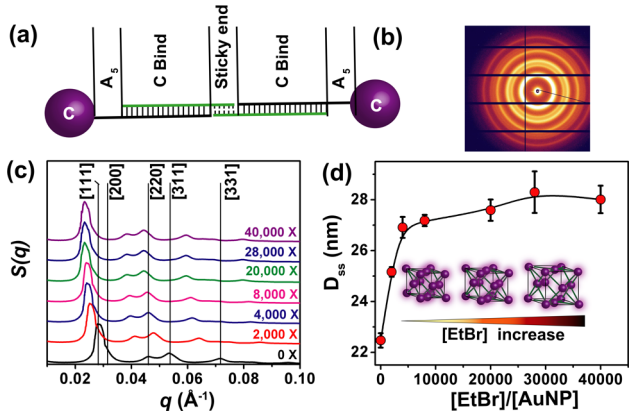

Figure 3. (a) NP linker design for fcc superlattice. (b) Representative SAXS pattern for fcc superlattice. (c) Evolution of the structure factor $S(q)$ for fcc superlattices with increasing excess of EtBr with respect to the particle concentration (25 nM). Peaks in $S(q)$ for native (without EtBr) superlattice are indexed as planes (as shown by black vertical lines and indexes) of fcc lattice. The shift of peaks to lower q indicates the increase in D_{CC}. See Figure S20 for enlarged view. (d) The surface-to-surface separations, D_{SS}, for the same system, as obtained from the SAXS measurements with respect to [EtBr]/[AuNP], where [EtBr] and [AuNP] are the concentrations of EtBr and AuNP, respectively.

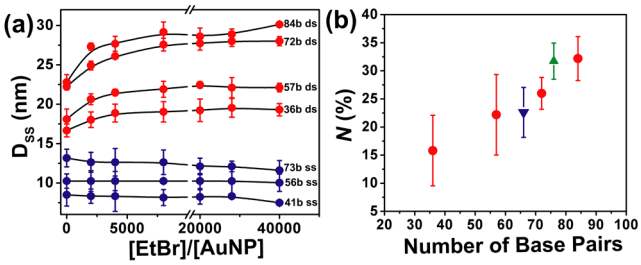

Figure 4. (a) Change of the D_{SS} calculated from SAXS measurements with respect to change of [EtBr]/[AuNP]. Systems rich in ds-DNA motifs are shown with red points, a total number of bp in the interparticle linking DNA is shown, and all the systems have same 20b ss-DNA region. Systems rich in ss-DNA motifs are shown in blue points, number of bases is as indicated and 6 bp ds fragment present for hybridization in all these systems. (b) A normalized maximum distance change, N (see text), for different ds-DNA rich bcc systems is plotted against the number of bp in in linking DNA. Green and blue triangles correspond to the fcc (76 bp ds-DNA and 10 b ss-DNA) and AlB_2 (66 bp ds-DNA and 20 b ss-DNA) systems, respectively.

typical SAXS pattern for fcc system is shown in Figure 3b. The diffraction peaks in the corresponding 1D pattern (black line in Figure 3c) are indexed as fcc lattice. Analogously to the bcc system discussed above, EtBr intercalation experiments with the fcc system revealed a similar behavior for the lattice constant. The evolution of structure factors with the increasing excess of EtBr is shown in Figure 3c. The initial interparticle distance measured from SAXS data, $D_{CC} \approx 27.5$ nm corresponded well with the estimated distance of 27.7 nm. The diffraction peaks shifted to lower q values without changing their relative positions, indicating a steady D_{SS} increase with preserved lattice symmetry. In Figure 3d we plot the D_{SS}, calculated from the SAXS data. D_{SS} increases from ≈22.5 to ≈ 28.0 nm around [EtBr]/[AuNP] ≈ 40000 and exhibits saturation behavior at higher EtBr concentrations. We fabricated AlB2 superlattices by mixing 10 nm A and B particles with same linker design as for bcc superlattice at 1:2 stoichiometry (see SI for sequence details). There is a total of 66 bp ds-DNA and 20 b ss-DNA motif separating A and B particles. We observed shift of diffraction peaks to lower q upon EtBr intercalation, indicating D_{SS} was increased from ≈24.3 to ≈29.8 nm at the saturation (see Figure S17).

In the next step, we examined the influence of EtBr on ds- and ss-DNA fragments in NP DNA shell. To study these aspects, we fabricated three additional bcc systems that are rich in ds-DNA motifs. Ten nm AuNPs were functionalized with ds-DNA spacers containing 36, 57, and 84 bp, along with 72 bp system described previously (details in SI). All the systems contained the same 20 bases ss-DNA fragment in the linking DNA. All four systems demonstrated bcc structure and were subjected to the detailed EtBr concentration studies using SAXS (see Figure S3−S6). We note that the 36 bp system showed a somewhat reduced order compared to the other systems, possibly due to the asymmetric design: particles A and B were functionalized with ss-DNA and ds-DNA-rich linkers, respectively (design details in SI). The D_{SS} for different bcc superlattices as a function of [EtBr]/]AuNP] is plotted in Figure 4a (red points). All systems exhibited isotropic expansion with the monotonic interparticle distance growth upon EtBr concentration increase, and D_{SS} reached a plateau at high EtBr concentrations.

We summarize the maximum normalized surface-to-surface distance change, N, for bcc superlattices with different ds-DNA in Figure 4(b) (red points), where $N = D_{SS}(40k) - D_{SS}(0)/D_{SS}(0)$ (DSS (40k) is D_{SS} at 40000 × [EtBr]/[AuNP] and $D_{SS}(0)$ is D_{SS} for the native superlattice). The obtained dependence of N on the length of ds-DNA motif (ss-DNA is 20 b for all four systems) is attributed to the reduced relative contribution of ss-DNA region for systems with larger duplexes. For example, we observed N ≈32% for 84 bp bcc superlattices vs ≈16% for 36bp, for which ss-DNA part is a larger fraction than for 84 bp system. Moreover, since ss-DNA is actually slightly contracts in the EtBr environment, as we discuss below, even somewhat larger N can be achieved for the systems with lower fraction of ss-DNA part. To illustrate that the normalized distance change is practically independent of the lattice type, we plot in Figure 4b, the magnitude of N for the AlB_2 system (blue triangle) and the fcc system (green triangle). The N demonstrated by the fcc and AlB_2 is indeed predominately determined by the length ds-DNA motifs, and these systems are in a good agreement with the trend obtained for bcc superlattice, implying that the approach can be used for the variety DNA-NP lattices.

To reveal the effect of EtBr on the ss-DNA regions, we created three superlattice systems that are rich in ss-DNA motif and contain a 6 base sticky end for the interparticle hybridization (see Figures S7−S10). We observed (Figure 4a, blue points) a milder response of D_{SS} with EtBr concentration increase for all systems. Moreover, in contrast to systems with a large fraction of ds-DNA (Figure 4a, red points), D_{SS} actually decreased by ∼3−8% at high EtBr concentrations. Since EtBr cannot intercalate into ss-DNA, the lack of distance increment was observed as expected. The observed decrease of ss-DNA length suggests that EtBr affects ss-DNA chain conformations, possibly, due the DNA charge screening, which consequently results in the persistence length reduction.

The reversibility of the interparticle distances upon EtBr removal was tested by washing the aggregates with *n*-butanol. By comparing the initial, intercalated and washed structures, we found that the intercalated EtBr could be fully removed from the aggregate due to the high solubility of EtBr in n-butanol after at least two washes (see Figures S14 and 15). Our SAXS

DOI: 10.1021/ja512799d
J. Am. Chem. Soc. 2015, 137, 4030−4033

experiments showed that scattering peaks were retained to the original q without changing the correlation length for the washed superlattices. Furthermore, *n*-butanol washed aggregates could be reused for further EtBr treatments, as shown in Figure S16. Such reversibility of lattice expansion and the lattice integrity for the intercalated and washed states demonstrate the robustness of the proposed approach.

Finally, we have explored the thermal stability of the EtBr-infused superlattices and compared it with the behavior of the native un-intercalated assemblies. EtBr intercalation has been shown to enhance the melting transition temperature of ds-DNA motifs, and it was of significant interest to examine if this effect could be translated to the DNA-NP superlattices. In order to investigate this aspect, we probed the melting temperature of a 72 bp bcc superlattice using dynamic light scattering (DLS) measurements and UV−vis spectroscopy, and monitored melting using SAXS. Both the DLS and UV−vis experiments indicate that the melting transition for EtBr-intercalated NP superlattice is elevated by ≈14 °C (see section 4 of SI and Figure S21a, b). In-situ SAXS reveled the structural changes with temperature (Figure S18). Accordingly, the obtained dependence of the correlation length, ξ, on temperature (Figure S21d) demonstrated that for DNA-NP superlattices intercalated with 20000 ×EtBr, ξ drastically decreased around 45 °C, contrary to the aggregates without EtBr, which melted around 33 °C. Thus, these findings demonstrate that EtBr intercalation is also advantageous for the thermal manipulation of DNA-NP systems without changing the DNA sequences and salt concentrations.

In summary, we have demonstrated that the lattice constants of DNA-NP superlattices can be effectively and reversibly controlled by the molecular intercalator, EtBr, which can increase the interparticle separations above 30%. We have further quantified the magnitude of this effect as a function of EtBr concentration as well as tested the applicability of this approach for different system designs and superlattice types. Our study also shows the predominant selectivity of EtBr to ds-DNA in comparison with ss-DNA. The excellent kinetics of lattice expansion (minutes) and its reversibility upon EtBr removal were observed. In addition, the enhanced thermal stability of the structure was revealed. Given that ds-DNA is the most abundant DNA form and is extensively used in nanotechnology, the demonstrated approach opens up exciting possibilities for the creation of dynamically tunable materials for regulating their functional responses. Besides that, a proper infusion of intercalating agents, which can be further controlled or cross-linked, might be a feasible route for post-assembly manipulation and processing of the nanomaterials created via DNA-driven assembly process.

■ ASSOCIATED CONTENT

Ⓢ Supporting Information

Experimental details, DNA sequences, additional data is provided. This material is available free of charge via the Internet http://pubs.acs.org.

■ AUTHOR INFORMATION

Corresponding Author

*ogang@bnl.gov

Notes

The authors declare no competing financial interest.

■ ACKNOWLEDGMENTS

This research was carried out at the Center for Functional Nanomaterials (CFN) and the National Synchrotron Light Source (NSLS), Brookhaven National Laboratory, by the U.S. Department of Energy, Office of Basic Energy Sciences, under contract no. DE-AC02- 98CH10886. S.P. and S.K.K. were supported by the US Department of Energy (DOE), Office of Basic Energy Sciences (BES), Division of Materials Science and Engineering under Award DE-FG02-12ER46909.

■ REFERENCES

(1) Tan, S. J.; Campolongo, M. J.; Luo, D.; Cheng, W. *Nat. Nanotechnol.* **2011**, *6*, 268−276.
(2) Pinheiro, A. V.; Han, D.; Shih, W. M.; Yan, H. *Nat. Nanotechnol.* **2011**, *6*, 763−772.
(3) Nykypanchuk, D.; Maye, M. M.; van der Lelie, D.; Gang, O. *Nature* **2008**, *451*, 549−552.
(4) Park, S. Y.; Lytton-Jean, A. K. R.; Lee, B.; Weigand, S.; Schatz, G. C.; Mirkin, C. A. *Nature* **2008**, *451*, 553−556.
(5) Macfarlane, R. J.; Lee, B.; Jones, M. R.; Harris, N.; Schatz, G. C.; Mirkin, C. A. *Science* **2011**, *334*, 204−208.
(6) Sun, D.; Gang, O. J. *Am. Chem. Soc.* **2011**, *133*, 5252−5254.
(7) Zhang, C.; Macfarlane, R. J.; Young, K. L.; Choi, C. H. J.; Hao, L.; Auyeung, E.; Liu, G.; Zhou, X.; Mirkin, C. A. *Nat. Mater.* **2013**, *12*, 741−746.
(8) Zhang, Y.; Lu, F.; Yager, K. G.; van der Lelie, D.; Gang, O. *Nat. Nanotechnol.* **2013**, *8*, 865−872.
(9) Kuzyk, A.; Schreiber, R.; Zhang, H.; Govorov, A. O.; Liedl, T.; Liu, N. *Nat. Mater.* **2014**, *13*, 862−866.
(10) Young, K. L.; Ross, M. B.; Blaber, M. G.; Rycenga, M.; Jones, M. R.; Zhang, C.; Senesi, A. J.; Lee, B.; Schatz, G. C.; Mirkin, C. A. *Adv. Mater.* **2014**, *26*, 653−659.
(11) Stuart, M. A. C.; Huck, W. T. S.; Genzer, J.; Müller, M.; Ober, C.; Stamm, M.; Sukhorukov, G. B.; Szleifer, I.; Tsukruk, V. V.; Urban, M.; Winnik, F.; Zauscher, S.; Luzinov, I.; Minko, S. *Nat. Mater.* **2010**, *9*, 101−113.
(12) Motornov, M.; Roiter, Y.; Tokarev, I.; Minko, S. *Prog. Polym. Sci.* **2010**, *35*, 174−211.
(13) Maye, M. M.; Nykypanchuk, D.; Cuisinier, M.; van der Lelie, D.; Gang, O. *Nat. Mater.* **2009**, *8*, 388.
(14) Kim, Y.; Macfarlane, R. J.; Mirkin, C. A. J. *Am. Chem. Soc.* **2013**, *135*, 10342−10345.
(15) Srivastava, S.; Nykypanchuk, D.; Maye, M. M.; Tkachenko, A. V.; Gang, O. *Soft Matter* **2013**, *9*, 10452−10457.
(16) Radha, B.; Senesi, A. J.; OBrien, M. N.; Wang, M. X.; Auyeung, E.; Lee, B.; Mirkin, C. A. *Nano Lett.* **2014**, *14*, 2162−2167.
(17) Xiong, H. M.; Sfeir, M. Y.; Gang, O. *Nano Lett.* **2010**, *10*, 4456−4462.
(18) Sebba, D. S.; Mock, J. J.; Smith, D. R.; LaBean, T. H.; Lazarides, A. A. *Nano Lett.* **2008**, *8*, 1803−1808.
(19) Tan, S. J.; Kahn, J. S.; Derrien, T. L.; Campolongo, M. J.; Zhao, M.; Smilgies, D.-M.; Luo, D. *Angew. Chem., Int. Ed.* **2013**, *53*, 1316−1319.
(20) Srivastava, S.; Nykypanchuk, D.; Fukuto, M.; Gang, O. *ACS Nano* **2014**, *8*, 9857−9866.
(21) Maye, M. M.; Nykypanchuk, D.; van der Lelie, D.; Gang, O. J. *Am. Chem. Soc.* **2006**, *128*, 14020−14021.
(22) Maye, M. M.; Nykypanchuk, D.; van der Lelie, D.; Gang, O. *Small* **2007**, *3*, 1678−1682.
(23) Ke, Y.; Bellot, G.; Voigt, N. V.; Fradkov, E.; Shih, W. M. *Chem.Sci.* **2012**, *3*, 2587−2597.
(24) Greschner, A.; Bujold, K.; Sleiman, H. F. *J. Am. Chem. Soc.* **2013**, *135*, 11283−11288.
(25) Coury, J. E.; McFail-Isom, L.; Williams, L. D.; Bottomley, L. A. *Proc. Natl. Acad. Sci. U.S.A.* **1996**, *93*, 12283−12286.
(26) Tsai, C. C.; Jain, S. C.; Sobell, H. M. *Proc. Natl. Acad. Sci. U. S. A.* **1975**, *72*, 628−632.

DOI: 10.1021/ja512799d
J. Am. Chem. Soc. 2015, 137, 4030−4033